CLM-R265

CLM-R265

UKAEA

Report

AN INVESTIGATION OF THE CONSTITUTION, STRUCTURE AND PROPERTIES OF SOME LOW ACTIVATION AUSTENITIC STAINLESS STEELS PROPOSED FOR FUSION

A. H. Bott
F. B. Pickering
G. J. Butterworth

CULHAM LABORATORY
Abingdon Oxfordshire
1986

C.18

Available from H. M. Stationery Office

Price £5.00

CLM-R265

AN INVESTIGATION OF THE CONSTITUTION, STRUCTURE AND PROPERTIES OF SOME LOW ACTIVATION AUSTENITIC STAINLESS STEELS PROPOSED FOR FUSION

A H Bott and F B Pickering
Department of Metals and Materials Engineering
Sheffield City Polytechnic, Sheffield S1 1WB

and

G J Butterworth
Culham Laboratory, Abingdon, Oxon., OX14 3DB
(Euratom/UKAEA Fusion Association)

ABSTRACT

An earlier study identified a number of possible high manganese, high nitrogen compositions as potential low-activation replacements for austenitic stainless steels of the types AISI 316, 320, 321 and FV548. In the present work, experimental casts of five proposed alloys were prepared and subjected to initial investigation of their microstructural constitution, phase stability and basic mechanical properties. With appropriate solution treatment it was possible to obtain fully austenitic constitutions for all the alloys. Ageing of material solution treated at 1150°C led to a limited degree of hardening at 400°C, mainly by precipitation of $M_{23}C_6$, and to a much greater degree of hardening by Ta(C,N) at test temperatures of 650° and 900°C. Precipitation hardening was most pronounced in the alloys having Ta:(C+N) ratios closest to stoichiometry for the relevant precipitate and, in the alloys with highest Ta contents, a Fe_2Ta Laves phase with needle-like morphology was observed to precipitate and subsequently spheroidise on prolonged ageing at 900°C. Transformation to σ phase only occurred on ageing at 650°C and then only at times greater than 100h and in alloys containing δ ferrite after solution treatment. The steels showed high stability toward martensite transformation under deformation and refrigeration. Room temperature 0.2% proof stress values of 470-610 MPa and tensile strengths of 750-1000 MPa were obtained and a high tensile ductility was observed. The fatigue resistance was found to be similar to that of the analogous commercial steels but the creep rupture strength was lower than expected.

April 1986

ISBN 085311 1480

CONTENTS

1. INTRODUCTION

An earlier study was performed in a previous phase of this work[1], based on published information, to establish the feasibility of designing reduced-activation austenitic stainless steels that could replace the conventional stainless steels of grades AISI 316, 320 and 321, and also the proprietary steel FV548, for use in first wall and breeder blanket components in fusion reactors. The alternative compositions were designed such that the contact γ-dose rate of post-service first wall material from a power reactor would not exceed 2.5×10^{-5} Svh^{-1} following a nuclear decay period of 100 years. This criterion should allow relatively safe handling of replaced components for subsequent recycling[2].

The basic philosophy adopted in the metallurgical design of the alternative alloys involved the replacement of those elements giving rise to high residual γ dose rates by elements showing more rapid rates of decay while at the same time maintaining the fully austenitic structure in conjunction with transformation characteristics and mechanical properties equivalent to those of the conventional austenitic stainless steels. In particular, the following major replacements were proposed:-

(1) Ni by Mn-N combinations
(2) Mo by W
(3) Ti and Nb by Ta.

Whilst the ferritic steels exhibit a greater resistance to radiation damage than the austenitic stainless steels, especially as regards void swelling, they have disadvantages in respect of their formability, weldability and ferromagnetic properties and may not differ greatly in terms of their overall embrittlement behaviour. In view of the expected scale and frequency of the replacement of first wall and blanket components, formability and weldability could be major factors favouring the use of the austenitic stainless steels.

The compositions proposed in the feasibility study[1] for the low activation austenitic stainless steels were assessed in terms of:-

(1) The constitution with respect to the austenite:ferrite ratio, which is particularly relevant to weldability, hot fabrication and

embrittlement effects during ageing

(2) The phase stability with respect to the transformation of austenite to martensite and the precipitation of sigma and other phases

(3) General cold working and formability

(4) Void swelling characteristics

(5) Mechanical properties and creep resistance.

In terms of these criteria, the proposed alternative alloys were predicted to have very similar characteristics to the conventional austenitic steels that they were designed to replace and, in particular, were predicted to have higher proof stress values and tensile strengths, largely as a consequence of the increased nitrogen content.

This paper describes and presents the results of an experimental appraisal of the actual constitutions, phase stability and mechanical properties of a selection of the proposed alloys, with the objective of validating the suitability of the compositions suggested.

2. EXPERIMENTAL OBSERVATIONS

The five experimental alloys for investigation were manufactured to compositions designed as alternatives to the AISI grades 316, 320 and 321, to the proprietary Firth Vickers alloy FV548 and, additionally, a composition OPTSTAB that was designed to have maximum austenite stability in terms of a fully austenitic constitution on cooling from high temperatures. The actual compositions of these experimental alloys are listed in Table 1. All alloys were prepared as 10kg vacuum casts using reasonably high purity raw materials, then hot-rolled to 20mm thick strip in 4 passes with inter-pass reheating at 1150°C.

2.1 Constitution and microstructure

Subsequent to hot-rolling, samples of the 5 alloys were solution treated for 30 minutes at temperatures in the range 1000°C to 1250°C at 50°C intervals, and then water-quenched to provide material for the assessment of the constitution in terms of the austenite:ferrite ratio.

Table 1 Compositions of experimental low activity austenitic stainless steels

Alloy type	Composition, mass percent						
	C	Mn	Si	Cr	W	Ta	N
Replacement 316 (316T)	0.038	14.49	0.17	16.30	4.10	1.35	0.259
Replacement 320 (320T)	0.050	14.80	0.18	17.70	4.22	0.76	0.415
Replacement 321 (321T)	0.060	11.90	0.16	17.60	1.00	0.68	0.432
Replacement FV548	0.053	12.26	0.17	16.40	2.20	1.50	0.269
Optimised stability (OPTSTAB)	0.070	11.90	0.19	14.20	2.15	0.50	0.285

Table 2 and Fig.1 indicate the stability of the austenite in the experimental alloys with respect to the formation of δ ferrite at solution treatment temperatures in the range 1000°-1250°C.

Table 2 Volume percentage of δ ferrite in solution treated alloys

Solution treatment temperature (°C)	Alloy				
	316T	320T	321T	FV548T	OPTSTAB
1000	0	0	0	0	0
1050	0	0	0	0	0
1100	7	0	0	8	0
1150	15	0	0	10	0
1200	42	0	9	31	0
1250	48	0	0	42	0

Exposure to temperatures in the range 1000° to 1250°C for 30 minutes showed that the 316T and FV548T alloys had the lowest austenite stability with respect to a fully austenitic constitution, both of these alloys being found

to contain δ ferrite at temperatures of 1100°C and above. The volumetric proportion of δ ferrite produced by a solution treatment of 30 minutes at 1100°C was in both cases less than 10%, though the proportion increased quite rapidly up to almost 50% at a temperature of 1250°C.

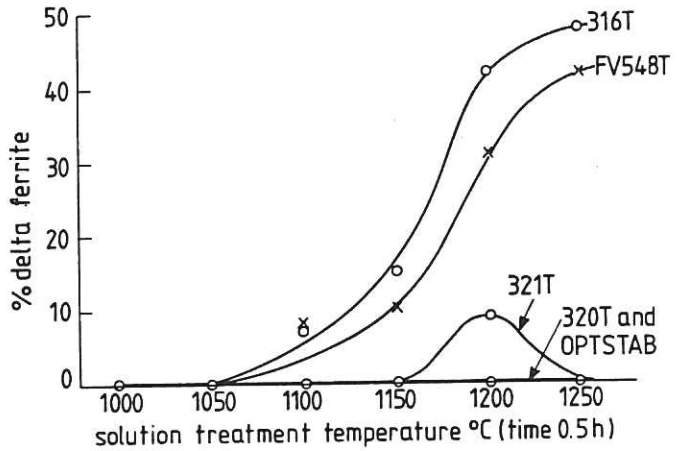

Fig.1 Effect of solution treatment temperature on the constitution of the replacement alloys in relation to the δ ferrite content.

All five alloys exhibited fully austenitic structures subsequent to solution treatment at temperatures of 1050°C or less. In the case of alloy 320T and the optimum stability alloy OPTSTAB, austenite stability extended over the full range of temperatures, while alloy 321T showed the presence of δ ferrite at only one temperature, namely 1200°C. At this temperature almost 10% δ ferrite was formed in alloy 321T, though solution treatment at 1250°C produced no detectable δ ferrite. No explanation can at present be offered for the fact that the 321T alloy contained δ ferrite only at 1200°C.

The resistance of the alloys to the formation of δ ferrite was found broadly to follow the trends that would be expected from consideration of a Schaeffler diagram of the type shown in Fig.2[3]. In fact the austenite stability of these alloys was found to correspond more closely to predictions made on the basis of the conventional Schaeffler diagram used for the Cr-Ni austenitic stainless steels, than to predictions based on a modified Schaeffler diagram, shown in Fig.3, recently proposed specifically for use with Cr-Mn stainless steels [4].

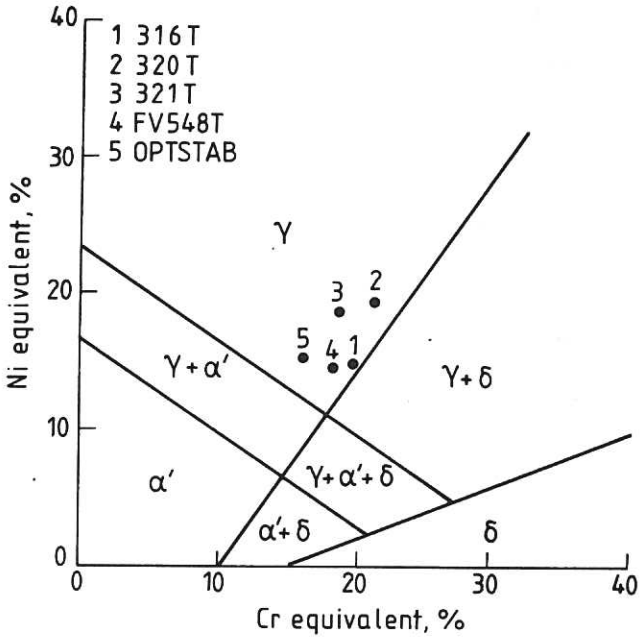

Fig.2 Compositions of the replacement alloys and predicted constitutions according to the standard Schaeffler diagram.

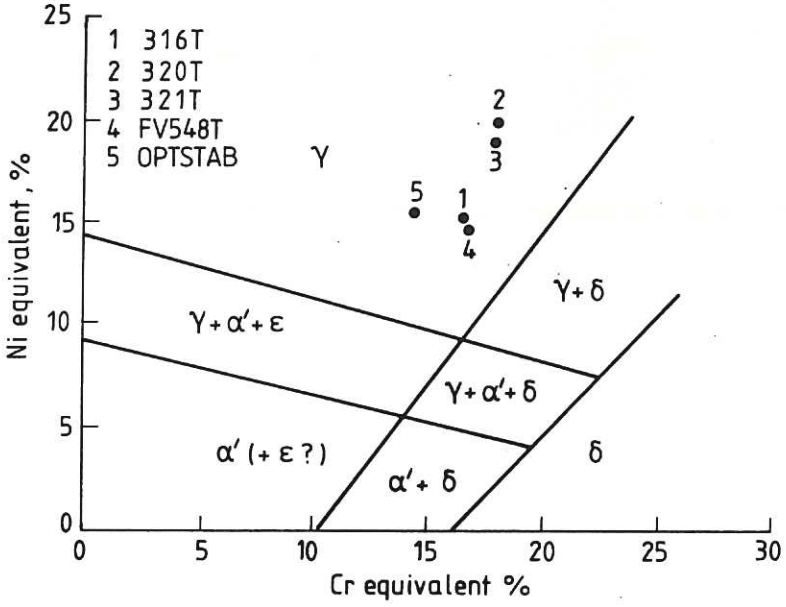

Fig.3 Compositions of the replacement alloys and predicted constitutions according to a modified Schaeffler diagram for use with Cr-Mn austenitic steels.

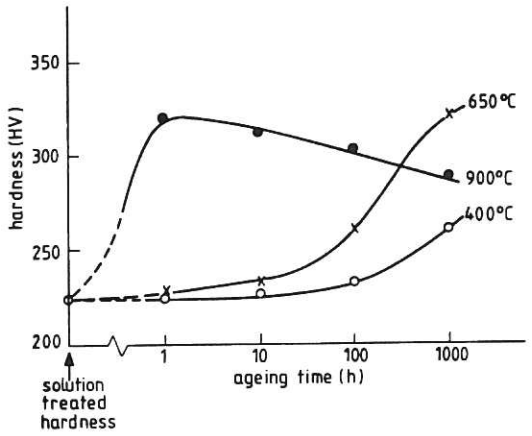

Fig.4 Age hardening effects in replacement alloy 316T.

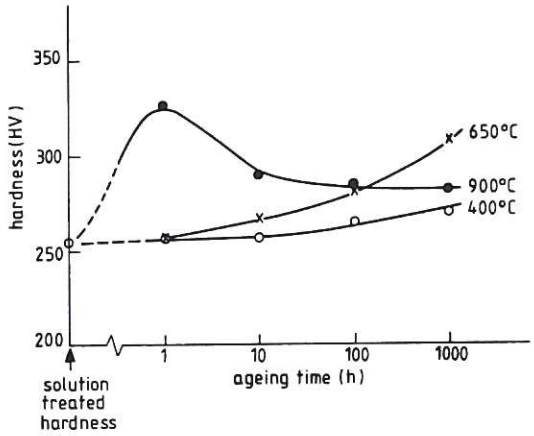

Fig.5 Age hardening effects in replacement alloy 320T.

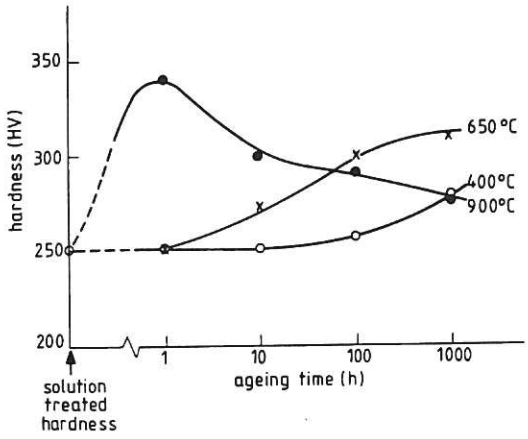

Fig.6 Age hardening effects in replacement alloy 321T.

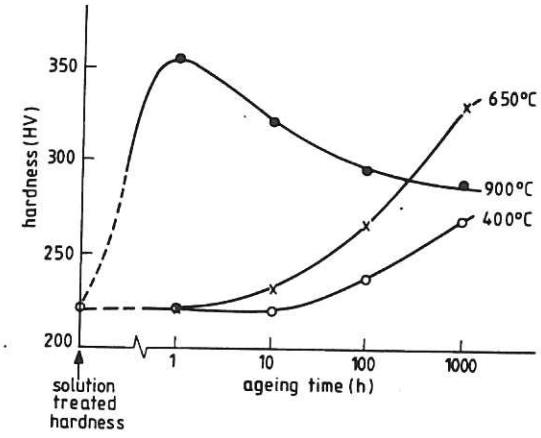

Fig.7 Age hardening effects in replacement alloy FV548T.

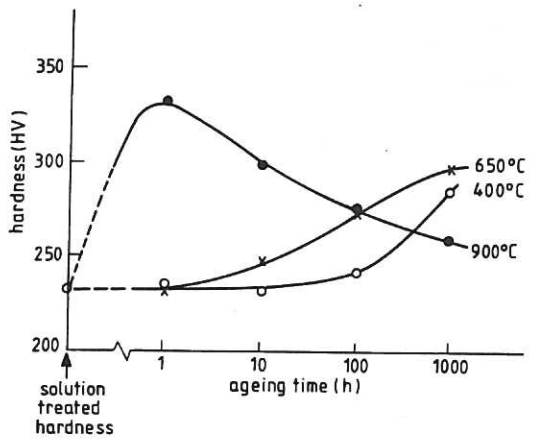

Fig.8 Age hardening effects in OPTSTAB alloy.

2.2 Effects of ageing

For each of the alloys, material from the sample that had received solution treatment at 1150°C was subjected to ageing at temperatures of 400°C, 650°C and 900°C, for times up to 1000h. The progress of the ageing process was followed by monitoring the changes in hardness of the alloys and the results are shown in Figs.4-8. Optical and electron microscopy was used to observe the microstructural changes during ageing. Transmission and scanning transmission electron microscopy, coupled with X-ray energy dispersive analysis to provide microanalytical data, were performed using a JEOL 100CX electron microscope with an EM-ASID - 4D STEM system, in conjunction with an EDAX 711 unit. Scanning electron microscopy was performed using a Phillips PSEM 500 microscope, coupled to a Link 860 analyser.

The techniques for preparing thin foils for the transmission microscopy examinations were the standard ones used for austenitic stainless steels. Rods were machined from samples of the alloys, from which thin discs were cut off. These were then dished and electropolished in a Struers 'Tenupol' apparatus until perforation occurred, using a solution of 5% perchloric acid in acetic acid operating at 60 volts and 0.13 amps.

The initial hardness values of the solution treated alloys were largely dependent on the amount of nitrogen in solution, despite the presence of δ ferrite in the FV548T and 316T alloys which, as shown by Fig.9, actually had the lowest hardness values. Alloy 320T had the highest solution treated hardness.

At 400°C ageing was found to cause little change in hardness until times in the range 100 to 1000h had elapsed and even then an increase in hardness of only 30HV was observed. This hardening effect was found to be related to a limited precipitation of carbides, predominantly of the $M_{23}C_6$ type. The relative extent of such precipitation hardening was observed to increase generally with increasing carbon content of the steel thus, for example, the optimum stability alloy increased in hardness more than alloy 320T. No sigma phase was observed in any of the materials after ageing at 400°C for times up to 1000h.

Ageing at the intermediate temperature of 650°C resulted in the expected

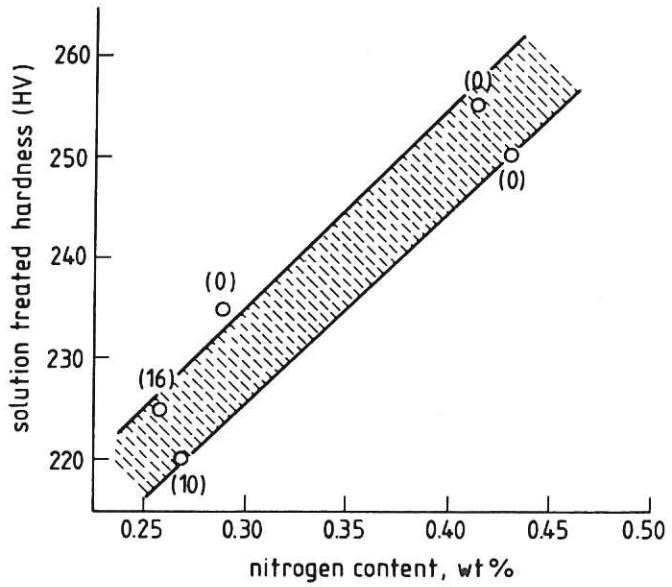

Fig.9 Effect of nitrogen content on the solution treated hardness. The numbers in brackets indicate the percentage of δ ferrite.

increase in both the degree and the rate of hardening in all five alloys.

This higher temperature promoted the precipitation of a Ta(C,N) phase rather than $M_{23}C_6$. In fact, the relative age hardening of the alloys FV548T and 316T, with Ta and (C+N) concentrations closest to the stoichiometric ratio, assuming approximately equal proportions of C and N in the Ta(C,N), was observed to be higher than for those alloys containing lower Ta contents.

After ageing at 650°C the alloys 316T and FV548T, both of which contained δ ferrite, were also found to have undergone a partial transformation to sigma phase, though this only commenced after 100h. In fact, alloy 316T contained only about 2% sigma phase after 10h, though the proportion increased to almost 10% after 1000h. On the other hand, FV548T contained about 2% and 9% sigma phase, respectively, for the same ageing treatments. This effect corresponds to the well known acceleration of the transformation to sigma phase by increased nucleation at the interface between austenite and any δ ferrite present[5]. More importantly, the alloys that did not contain δ ferrite after prior solution treatment remained resistant to sigma phase formation for exposure times to at least 1000h. In alloys 316T and FV548T an intragranular, needle-like precipitate was also noted, initially thought to be Cr_2N. Subsequent EDX analysis showed the phase to be more probably Fe_2Ta Laves phase surrounded by a chromium-enriched matrix.

Ageing at 900°C caused the hardness of each alloy to increase for times up to 10h, followed by overaging at longer times. This effect was observed to be due to the formation of Ta(C,N) precipitates and to their coarsening with time. No sigma phase was detected in any of the alloys at this ageing temperature but some Fe_2Ta was observed in alloys 316T and FV548T. This Fe_2Ta showed progressive spheroidisation as the ageing time increased above 10-100 hours. It should be noted that 900°C is generally regarded as being above the maximum temperature at which sigma phase forms in Fe-Cr-Ni alloys.

2.3 Transformation to martensite

Two aspects of the stability of the austenite in relation to its susceptibility to a martensitic transformation have been examined, namely the effect of cold work and the effect of refrigeration. Material that had been solution treated at 1150°C was cold rolled at room temperature to a reduction of 10% to enable a study to be made of austenite stability in terms of the resistance to a deformation-induced transformation to martensite. Refrigeration of 1150°C solution treated material in liquid nitrogen for 24h provided samples for an examination of the stability of the austenite with respect to its transformation to martensite at low temperature.

Transmission electron microscopy of 10% cold worked material from the experimental alloys revealed similar structures for all five steels, namely banded structures comprising deformation twins, stacking faults and h.c.p. ε martensite, as illustrated by Fig.10. Not only do these features have very similar morphologies but it is also impossible to distinguish between the three features in most of the f.c.c. matrix orientations on account of the overlapping of the features in the image and in the electron diffraction patterns, complicated in some cases by missing second phase reflections[6]. For these reasons it was not possible to determine unambiguously the relative fractions of the individual structural features. Moreover, it is considered likely, as has been proposed for other stainless steels having low stacking fault energies, that the ε martensite may result from nuclei consisting of overlapping stacking faults[7], thus confusing the transition between these two features.

It was noted qualitatively that the proportion of ε martensite and stacking faults was higher in the alloys 316T and 320T than in the other three alloys,

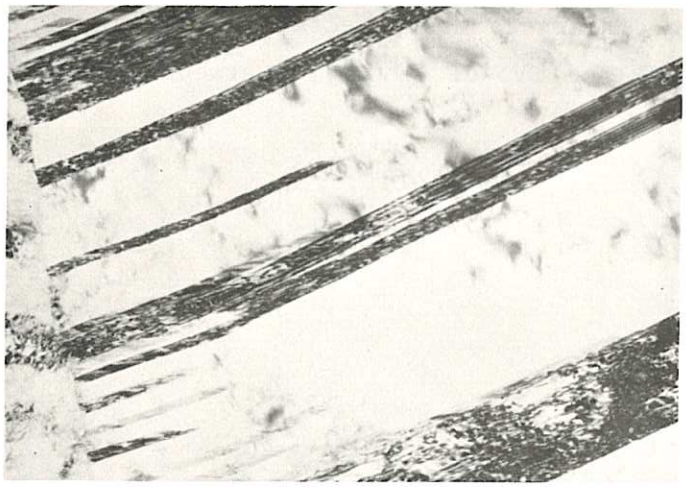

(a) Alloy 320T, mag. 40,000 showing stacking faults and ε martensite

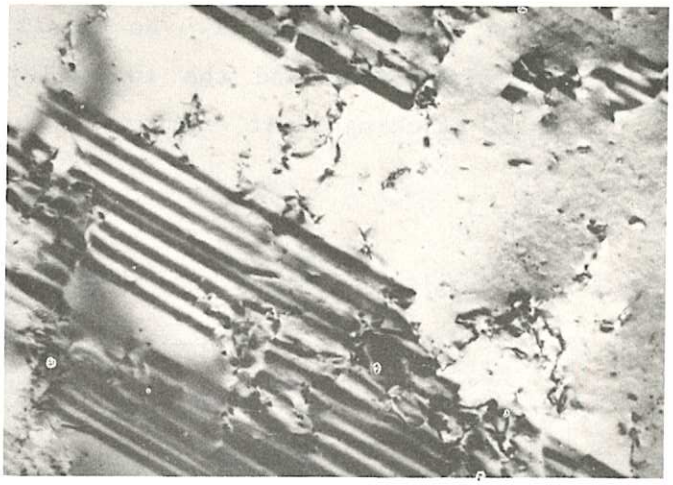

(b) Alloy FV548T, mag. 75,000 showing mainly stacking faults, some overlapping possibly to form ε martensite

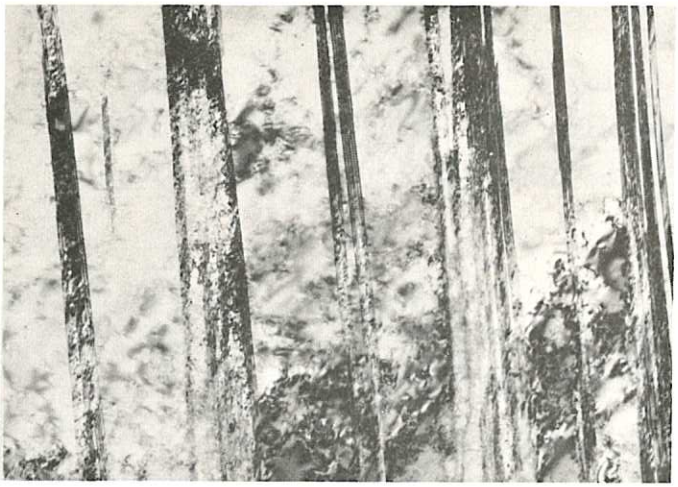

(c) OPTSTAB alloy, mag. 40,000 showing deformation twins, stacking faults and ε martensite

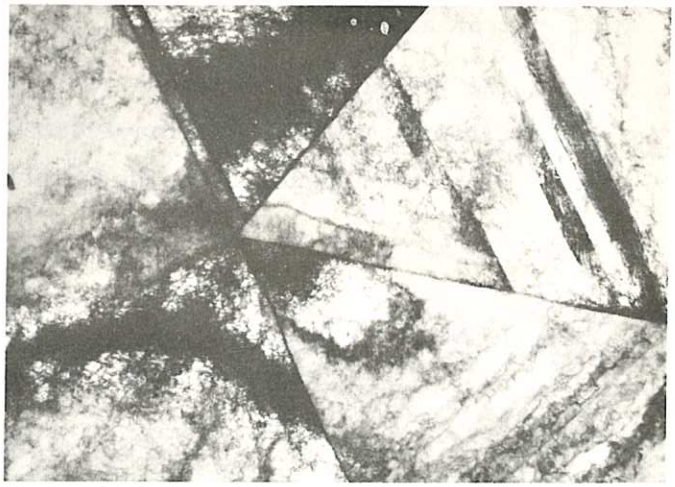

(d) OPTSTAB alloy, mag. 15,000 showing annealing twins and possibly ε martensite

Fig.10 Typical electron micrographs of the alloys following 10% deformation at room temperature.

as in fact would be predicted from the calculated relative stacking fault energies, shown in Fig.11. No significant difference was detectable between the OPTSTAB alloy and the two alloys 321T and FV548T having intermediate relative stacking fault energies.

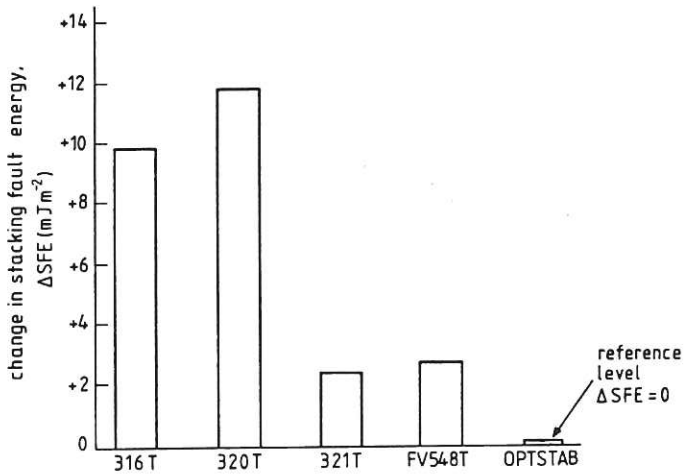

Fig.11 Calculated stacking fault energy (SFE) relative to that of the optimum stability alloy OPTSTAB, which had the lowest calculated SFE of all the replacement alloys.

Since the predictive equations previously employed[8] to indicate the likely susceptibility to deformation-induced martensite were based on data for α' rather than ε martensite, no correlation can be drawn between the predictions

Table 3 Susceptibility to martensite transformation (relative to the optimum stability alloy)

Alloy	start ΔMd_{30}(°C)	ΔM_s (°C)
316T	-22	-1
320T	-122	-224
321T	-109	-214
FV548T	-17	+2
OPTSTAB	0	0

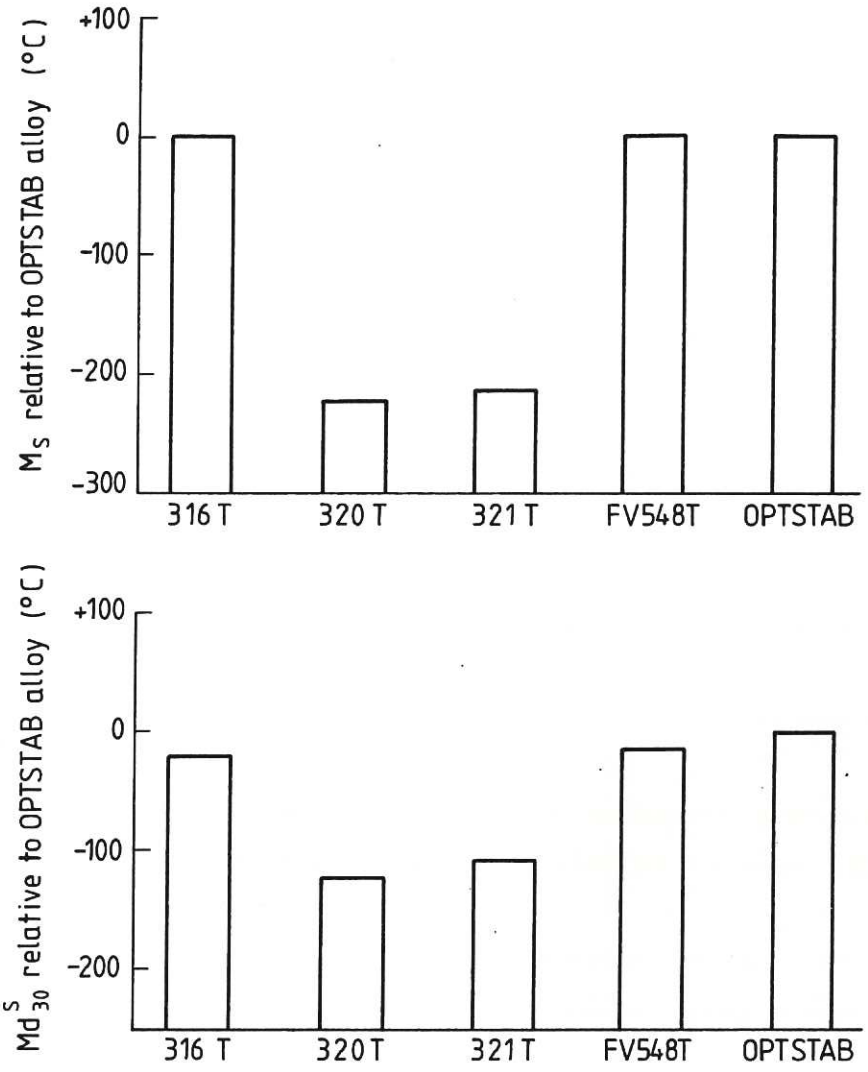

Fig.12 Calculated α' martensite M_s and Md^S_{30} temperatures for the replacement alloys relative to the values for the optimum stability alloy OPTSTAB.

and the actual response of the alloys to 10% cold work deformation. The predicted relative α' martensite start temperatures and the relative M_d temperatures are listed in Table 3 and shown diagrammatically in Fig.12 . It is considered, however, that greater amounts of cold work would probably induce transformation to α', possibly more rapidly than the predicted values might suggest in view of the nucleation effect of pre-existing ε martensite.

By contrast, refrigeration to -196°C in liquid nitrogen produced α' martensite as well as the ε phase, as shown by Fig.13. The extent of the transformation to α' martensite varied between different positions within each sample, making measurement of the volume fractions difficult. It was clear, however, that after 24h at -196°C the alloys 316T, FV548T and OPTSTAB contained similar volume fractions of α' martensite and that these alloys contained more α' martensite than did the 320T and 321T alloys. This observation agrees with the trend predicted by the calculated M_s temperatures given in Table 3 and Fig.12.

2.4 Tensile testing

Tensile tests were conducted at both room temperature and 500°C. Tensile specimens were strained to failure using an Instron TT-CM testing machine at a crosshead speed of 5mm s^{-1}. The load was measured using a 5000kg load cell linked to a potentiometric recorder. The extension was measured by means of a strain gauge extensometer linked to the potentiometric recorder, to permit the calculation of true stress and true strain and thereby determine work hardening rates and maximum uniform elongations. True stress-true strain curves were determined by standard methods. A three-zone tube furnace was employed to facilitate the testing at an elevated temperature of 500°C.

2.4.1 Room temperature tensile properties

The results of tensile testing after solution treatment at 1150°C provided data on the 0.2% proof stress and tensile strength and gave some indication of the likely cold formability, in terms of the elongation, reduction of area and work hardening rate, of the five replacement alloys.

The 0.2% proof stress values are listed in Table 4 and were compared with the values predicted by calculation[8] using the actual compositions of the

(a) Alloy 320T, mag. 100,000 showing α' martensite laths with ε martensite or overlapping stacking faults

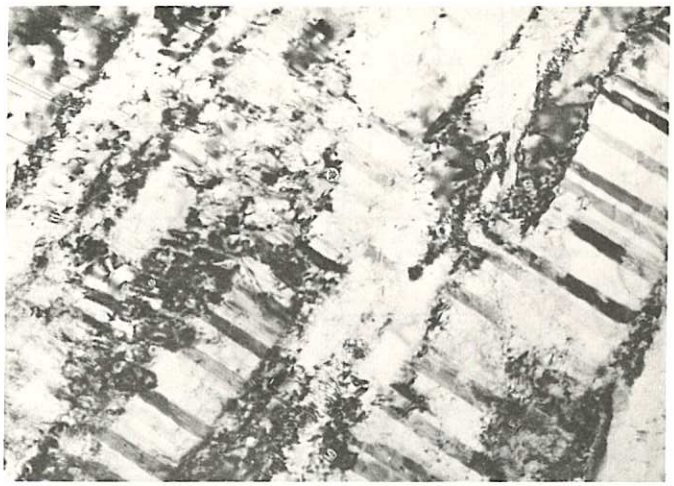

(b) Alloy FV548, mag. 50,000 showing α' martensite with stacking faults or ε martensite between α' laths

(c) Alloy FV548T, mag. 75,000 showing α' martensite laths with stacking faults or ε martensite between the α' laths

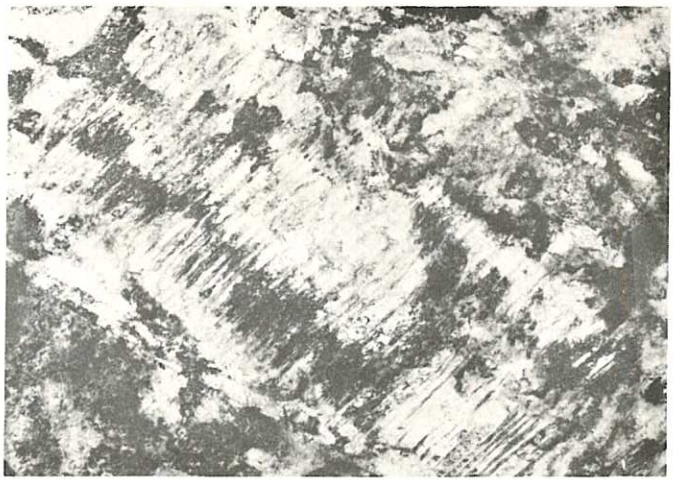

(d) OPTSTAB alloy, mag. 30,000 showing α' martensite and ε martensite

Fig.13 Typical electron micrographs of the replacement alloys after refrigeration at -196°C for 24h.

Table 4 Mechanical properties - tensile data at room temperature

Alloy	0.2% proof stress MPa	U.T.S. MPa	% elong.	% R of A	Work hardening rate MPa
316T	581	807	39 (31)	54	265
320T	612	870	44 (36)	53	420
312T	512	768	49 (41)	68	439
FV548T	520	785	47 (39)	60	397
OPTSTAB	469	1006	62 (60)	42	658

Figures in brackets indicate the maximum uniform elongation.
Work hardening rate measured at a true strain of 0.2.

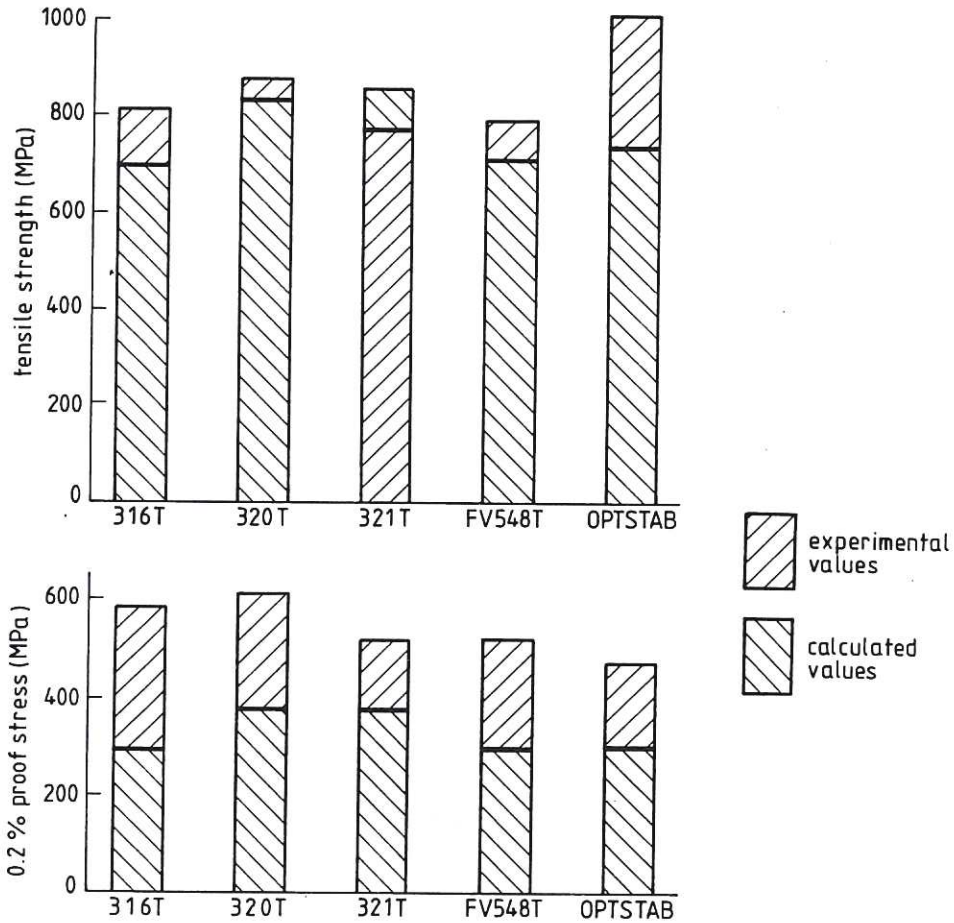

Fig.14 Comparison of calculated and experimental values of room temperature 0.2% proof stress and tensile strength for the replacement alloys.

replacement alloys and published equations of the type used in the feasibility study[1]. The predicted values were found in all cases to underestimate the actual results, as shown in Fig.14, though the relative proof stress values for the different alloys were very similar to those predicted. In fact all five alloys were considerably stronger than the analogous standard grades of stainless steel, mainly as a consequence of the solid solution strengthening by nitrogen, which was underestimated in the published equation. The proof stress values were exceeded by up to a factor of 2. Alloy 316T, for example, exhibited a 0.2% proof stress of 581 MPa, as compared with the 250-300 MPa typical of a standard AISI 316 grade.

A similar trend was also evident in the ultimate tensile strength values of the replacement alloys, as shown by Fig.14, which easily exceeded the predicted levels for all the compositions except 321T. The reason for the rather low tensile strength of 321T alloy may be associated with its considerably lower W content, as well as a rather low Ta content, with a consequent loss of solid solution strengthening. Tensile strength values ranging from about 770 MPa to over 1000 MPa were obtained. It should be pointed out, however, that even the relatively low strength of 768 MPa for alloy 321T compares favourably with the 500-600 MPa typical of standard AISI 321.

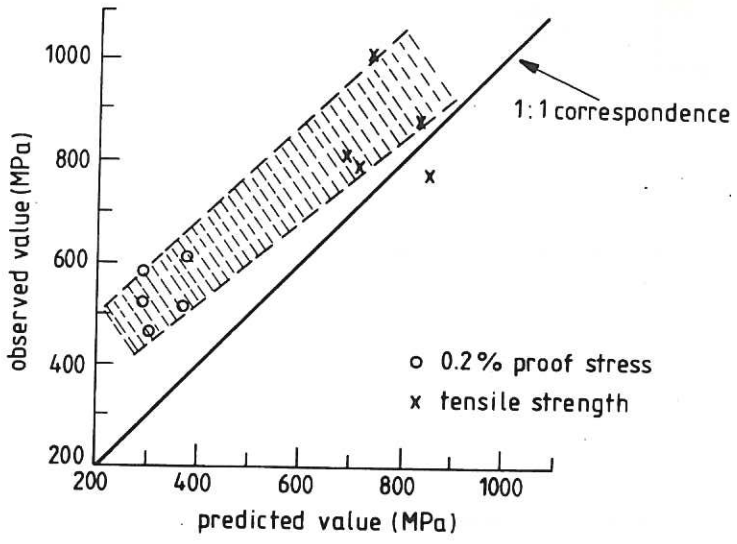

Fig.15 Predicted versus observed proof stress and tensile strength values at room temperature.

A comparison between the predicted and observed proof stress and tensile strength values is shown in Fig.15, from which it can be seen that whilst the predicted values were lower than the observed values, the difference was less for the tensile strength than for the proof stress.

Insufficient sample material was available for formability testing in the present study and this aspect will be investigated in future work. The likely forming characteristics of the experimental alloys may be inferred from the ductility parameters and the work hardening rates.

Reduction of area values for the replacement steels at room temperature were found to lie in the range 42% to 68%, while total percent elongation values ranged from 39% for alloy 316T to 62% for OPTSTAB, as can be seen from Table 4 and Fig.16. A typical value for standard AISI grades 316, 320 and 321, in the equivalent solution treated condition, would be 40% elongation. Such a value was equalled or exceeded, considerably so in the case of the optimum stability alloy, in the elementally substituted steels. In fact, more importantly with respect to formability, the percentage maximum uniform elongation, indicated in Table 4 and Fig.16, was generally high for all five alloys, ranging from 31% to 41% for 316T, 320T, 321T and FV548T but, significantly, up to 60% for the OPTSTAB alloy with its high work hardening rate.

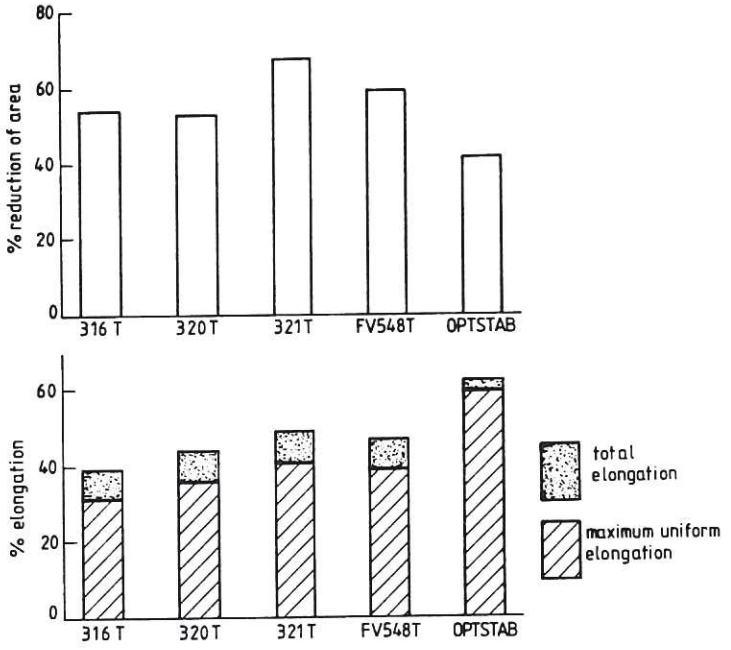

Fig.16 Values for room temperature tensile ductility of the replacement alloys.

The data obtained for work hardening rates at room temperature and at 0.2 true strain are presented in Table 4 and Fig.17, and ranged from 265 MPa for alloy 316T to 658 MPa for the optimum stability alloy. There appeared to be no existing data from which to predict the work hardening rates for the experimental steels. Figure 18, however, shows an inverse relationship between the work hardening rate and the predicted relative stacking fault energy[1,10]. This result indicates that the trends exhibited in the calculated values of the stacking fault energy are probably correct and also suggests that the stretch formability, which is improved by increasing the work hardening rate, will be satisfactory. The validity of this prediction will be tested in future investigations. The good correlation, shown in Fig.18, between the maximum uniform elongation and the work hardening rate is just what would be expected. In the case of OPTSTAB alloy, the combination of a relatively low proof stress, in comparison with the other four alloys, and a high maximum uniform elongation would appear particularly promising with regard to the stretch formability while the relatively high work hardening rate could offer the required high strength in a cold-worked component.

2.4.2 Tensile properties at 500°C

The results of measurements of proof stresses at the elevated temperature of 500°C are given in Table 5 and Fig.19 and confirm the high strength levels of

Table 5 Mechanical properties - tensile data measured at 500°C

Alloy	0.2% proof stress, MPa	U.T.S. MPa	% elong.	% R of A
316T	301	520	22 (17)	63
320T	354	617	38 (31)	56
321T	260	551	33 (25)	72
FV548T	268	535	29 (22)	67
OPTSTAB	227	525	42 (36)	62

Figures in brackets indicate the estimated maximum uniform elongation

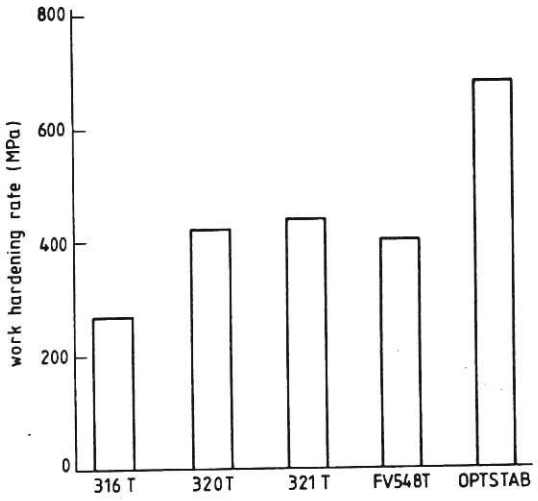

Fig.17 Work hardening rates at room temperature for the replacement alloys, measured at a true strain of 0.2.

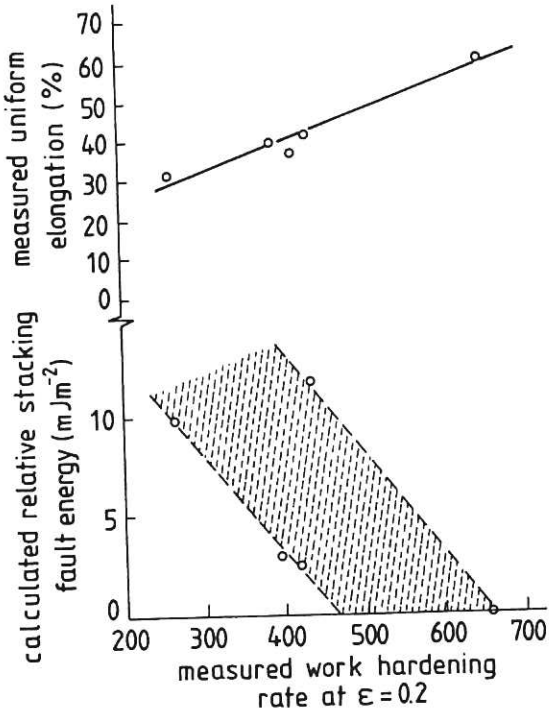

Fig.18 Relationships between measured work hardening rate, calculated relative stacking fault energy and uniform elongation.

the replacement alloys, the values ranging from some 230 MPa for the optimum stability alloy to over 350 MPa for alloy 320T. Compared with typical data for the standard AISI austenitic stainless steels[9], the proof stress values at 500°C were again about twice those for the standard steels. This result indicates a considerable degree of strength retention at elevated temperatures.

Tests at 500°C showed that the ultimate tensile strength remained high for all five replacement alloys at elevated temperatures, with the highest, for alloy 320T, exceeding 600 MPa and the lowest, for 316T, remaining above 500 MPa. The results are shown in Fig.19. The observed values may be compared with typical tensile strength values at 500°C of 400-500 MPa for standard AISI 316 and 321 stainless steels[9].

The tube furnace required for testing at the elevated temperature of 500°C prevented the use of the extensometer required to provide the true stress/true strain data necessary for the accurate determination of the maximum uniform elongation. For this reason the values for this parameter at 500°C are estimated from engineering stress/strain data and are given in Table 5 and Fig.19.

Ductility values at 500°C are also plotted in Fig.19 and range from 22% to 42% total elongation and 56% to 72% reduction of area. The estimated maximum uniform elongation values ranged from 17% for alloy 316T to 36% for the optimum stability alloy.

2.5 Creep behaviour

Creep testing was conducted on Denison T47E creep and stress rupture machines. The tests were necessarily short-term in nature, requiring a relatively high stress level of 185 MPa at the test temperature of 700°C to accelerate the creep rate and reduce rupture life. These creep test conditions were chosen because they enabled a comparison to be made with the results for a conventional Type 347 austenitic stainless steel, and the stress was not believed to be above the estimated 0.2% proof stress at 500°C of 200-250 MPa.

The rupture lives, indicated in Table 6 and Fig.20, ranged from 190h for the OPTSTAB alloy to 420h for FV548T. Comparison of these rupture lives with

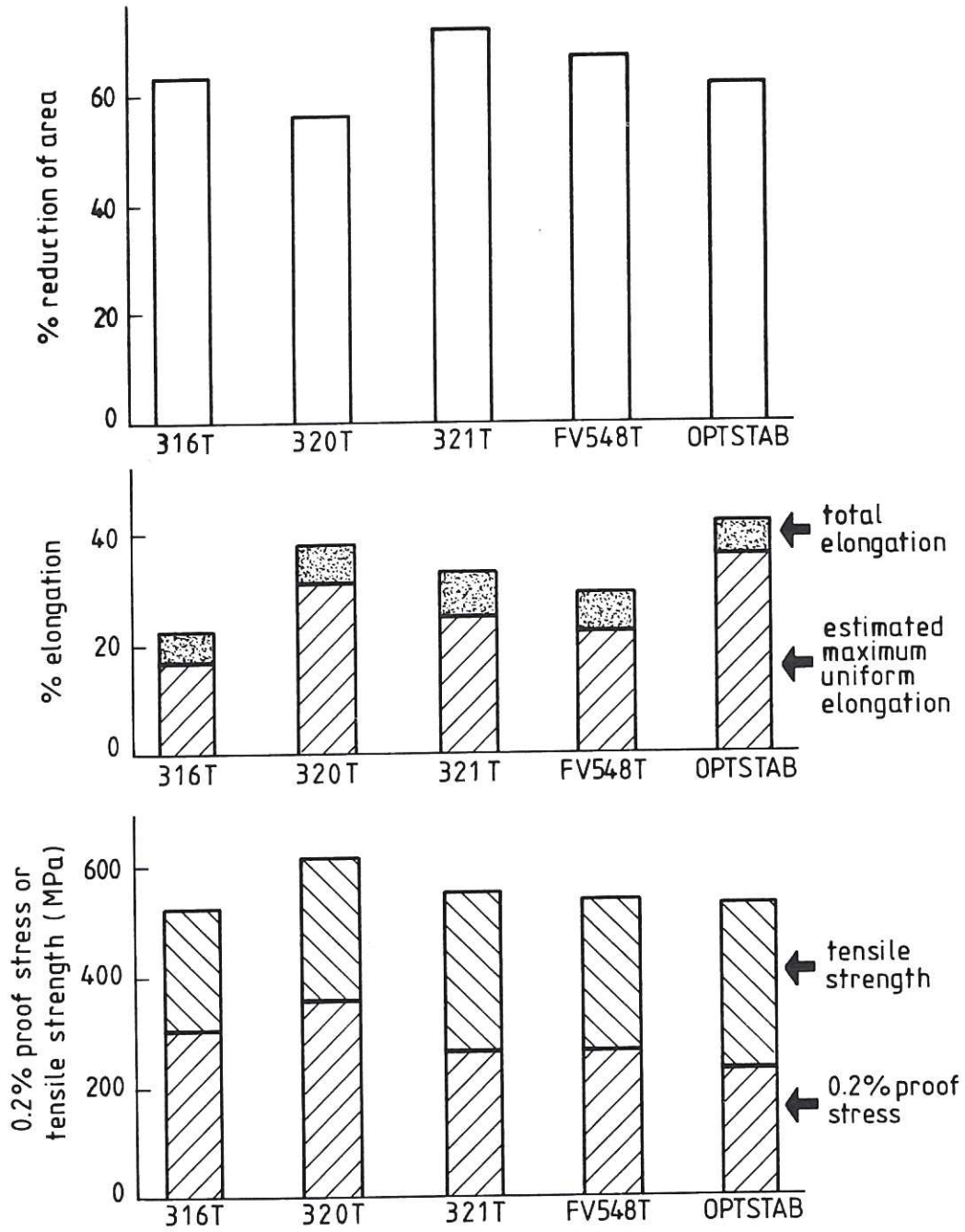

Fig.19 Tensile properties of the replacement alloys at 500°C.

those for 347 type steels containing Nb, with a Nb:C ratio close to stoichiometry, indicates that the replacement alloys, which contain Ta, had rather lower rupture lives than the 347 type steels, for which the rupture lives are estimated to be of the order of 1000 hours for identical test conditions[11]. It is notable that the optimum stability alloy exhibited by far the lowest rupture life, which correlates with the fact that it also had the lowest proof stress at 500°C. It is possible, therefore, that in the case of the optimum stability alloy the creep stress of 185 MPa was close to or even above the proof stress at the test temperature of 700°C.

Table 6 Creep properties - rupture life under a stress of 185MPa at a temperature of 700°C

Alloy	Rupture life (h)
316T	408
320T	284
321T	248
FV548T	420
OPTSTAB	190

It is significant that the two replacement alloys with Ta:(C+N) ratios closest to stoichiometry showed the greatest rupture lives. This finding indicates the influence of the precipitation of Ta(C,N) during the creep test on the rupture life. A similar conclusion has been drawn in published work with regard to NbC precipitation in 347 type steels[11]. It is, moreover, suggested that the rupture life of these replacement alloys may be further increased by:-

(a) ensuring a stoichiometric ratio of Ta:(C+N) in the alloy

(b) increasing the Ta and (C+N) contents of the alloy in the stoichiometric ratio, particularly if the solution treatment temperature is controlled to ensure complete solution of the Ta(C,N)

(c) by further increasing the Ta and (C+N) contents of the alloy to leave undissolved Ta(C,N) in the solution treated condition which, as shown in other work[11], is capable of increasing the creep rupture life.

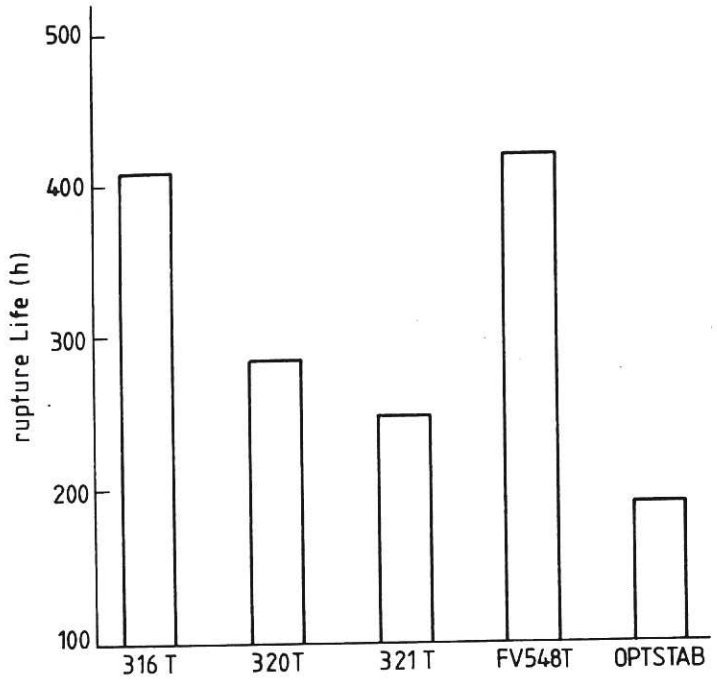

Fig.20 Creep rupture lives of the replacement alloys. The time to rupture at 700°C under a stress of 185 MPa is plotted.

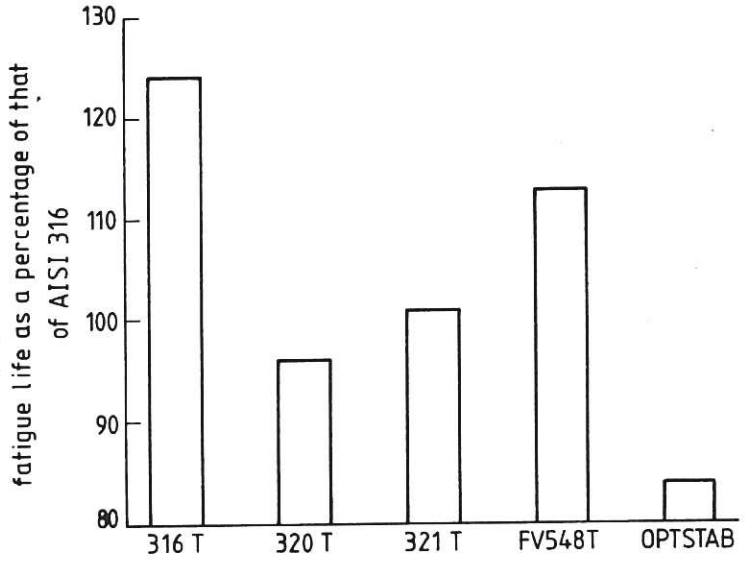

Fig.21 Fatigue lives of the replacement alloys expressed as a percentage of the fatigue life of standard AISI stainless steel tested at room temperature under identical conditions.

2.6 Fatigue life

Most current conceptual designs of fusion reactor feature a pulsed mode of operation and in this case thermal fatigue of the first wall and blanket structures would be a major design consideration. Components made of austenitic stainless steel would be susceptible to thermally-induced fatigue failures on account of the relatively high thermal expansion coefficient and rather low thermal conductivity of this material. In particular, the initiation stage of a fatigue crack varies considerably with the stress concentration and is dependent on the geometry of the component and the surface finish. Once a fatigue crack has been initiated, the propagation of that crack controls the fatigue life. Consequently, tests have been conducted on notched specimens, pre-fatigued so as to lead to crack initiation with a reproducibly-constant sharp fatigue crack at the microscopic level, which eliminates microscopic variations in notch acuity associated with variable machining conditions. Fatigue testing was undertaken on an E.S.H. ± 250kN, 4-column, servo-hydraulic test system using standard compact tension specimens, with W = 25 mm, ie. 31.25 mm x 30 mm x 12.5 mm and notch depth = 12.5mm, of the type employed for fracture toughness testing. W is the distance between the axis of loading and the un-notched rear surface of the specimen. Specimens were cycled with a constant amplitude in the load-controlled mode, maintaining a maximum load of 200 kN and imposing a triangular waveform for load reversals. All tests were performed at a cycling frequency of 10 Hz. The fatigue life thus determined was expressed relative to that for a solution treated conventional AISI 316 austenitic stainless steel tested under identical conditions.

The results of this assessment are presented in Table 7 and Fig.21, from which it can be seen that the relative fatigue lives ranged from 84% to 125% of that exhibited by the standard AISI 316 alloy, the extremes being represented by the OPTSTAB alloy and alloy 316T, respectively. While these results give some basis for comparison of the general fatigue behaviour of the replacement alloys, it should be remembered that in view of the temperature variations likely to be experienced by first wall materials an appreciation of the more complex phenomenon of creep-fatigue interaction under anticipated service conditions would be more appropriate.

Table 7 Fatigue properties - fatigue life as a percentage of the number of cycles to failure for AISI 316 steel tested under identical conditions

Alloy	Relative fatigue life (%)
316T	124
320T	96
321T	101
FV548T	113
OPTSTAB	84

2.7 Manganese depletion

It has previously been reported[12,13] that stainless steels containing high manganese concentrations may be susceptible to a reduction in austenite stability as a consequence of the evaporative loss of manganese from the surface of such materials when exposed to elevated temperatures under vacuum. The propensity for manganese loss by volatilisation from the surface was briefly investigated for the low-activation alloys. Samples of alloy 320T and OPTSTAB, representing the highest (~ 14.5%) and lowest (~ 12%) Mn levels of the experimental series, were subjected to a temperature of 650°C under a vacuum of 10^{-4} torr for 1000h. The extent of the Mn depletion was measured across a section taken at 90° to the sample surface, using a Phillips PSEM500 scanning electron microscope coupled with EDX microanalysis and X-ray mapping using a Link 680 analyser. The observations are illustrated by Fig.22.

Both alloys yielded very similar results and these showed that the loss of manganese was restricted to a surface layer of up to 0.01 mm in depth, which had experienced a maximum diminution in the manganese concentration amounting only about to 1.5%. It is considered that the extent of this loss of manganese should not significantly de-stabilise the overall structure of the replacement alloys.

(a) X-Ray Image - Mn radiation

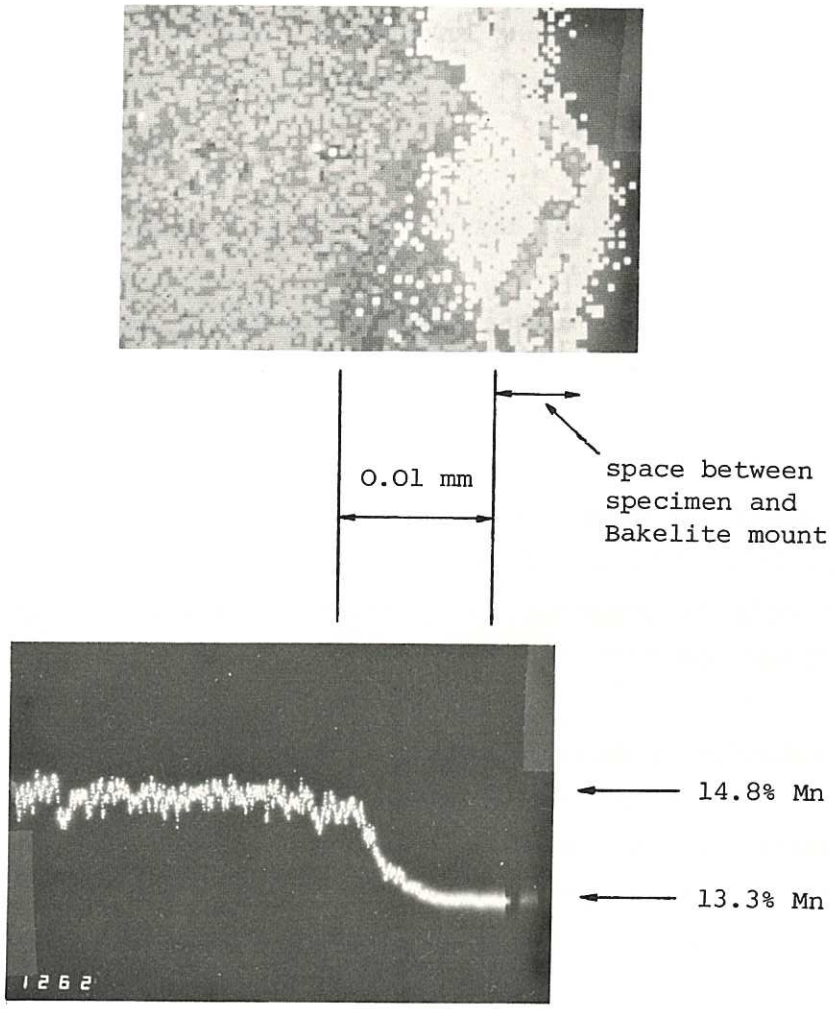

(b) Line Scan - Mn radiation

Fig.22 Observations on manganese depletion at the surface of the highest Mn alloy, 320T, after 10^3h at 650°C in a vacuum of about 10^{-4} torr.

3. CONCLUSIONS

A series of experimental observations and measurements has been performed to test the results of the earlier feasibility study, which predicted the constitution, microstructural characteristics and various mechanical properties of a series of proposed low-activity alloys as replacements for standard austenitic stainless steels in fusion reactor first wall and blanket applications.

The following general conclusions may be drawn from the experimental work:-

(1) It was possible, using an appropriate solution treatment temperature, to obtain a fully austenitic constitution for all the replacement alloys. For alloy 320T and the optimised stability alloy OPTSTAB the austenitic structure extended over the full range of solution treatment temperatures, from 1000°C to 1250°C. For alloys 316T, 321T and FV548T, however, fully austenitic structures could only be produced using solution treatment temperatures of 1000°C to 1050°C.

(2) The relative stability of the austenite with respect to delta ferrite formation was observed to follow the general trends indicated by the standard Schaeffler diagram but could not be accurately predicted by such a diagram. A recently proposed version of the Schaeffler diagram developed specially for Cr-Mn austenitic steels appeared, however, to be less successful than the conventional Schaeffler diagram in predicting the constitution of the tailored alloys.

(3) Ageing of 1150°C solution treated material led to precipitation hardening of the replacement alloys to a limited degree at 400°C, predominantly by $M_{23}C_6$, and to a much greater extent by Ta(C,N) at test temperatures of 650°C and 900°C.

(4) Precipitation hardening effects were most pronounced in those alloys in which the Ta:(C+N) ratio was closest to the stoichiometric ratio for the observed precipitate.

(5) In the alloys containing the highest Ta contents, a needle-like Fe_2Ta Laves phase was seen to precipitate and subsequently spheroidise on prolonged ageing at 900°C.

(6) Transformation to sigma phase only occurred on ageing at 650°C and then only at times of more than 100h and only in alloys that contained δ ferrite after solution treatment.

(7) Cold working to 10% resulted in a strain-induced transformation to ε martensite, to a degree that confirmed the trend expected from the calculated relative stacking fault energies, ie. a higher proportion being formed in those alloys with the lowest relative stacking fault energy.

(8) Refrigeration at -196°C for 24h resulted in a transformation to α' martensite to an extent that followed the trend indicated by the calculated values of M_s.

(9) The 0.2% room temperature proof stress values of all five alloys considerably exceeded the predicted values, by up to a factor of 2, though their relative values were broadly as indicated by the predictions from the published equations.

(10) Room temperature ultimate tensile strength levels exceeded the predicted values in all except one case and again the trend in relative strength levels was similar to that shown by the predicted values.

(11) The percentage elongation and percentage reduction of area values for the replacement alloys at room temperature and at 500°C equalled or exceeded the values quoted for the standard AISI grades of steel.

(12) Maximum uniform elongation values at room temperature and at 500°C were generally good for all five alloys and especially so for the optimum stability alloy.

(13) The 0.2% stress values remained high at elevated temperature (500°C), at a level approximately twice that of standard AISI grades.

(14) Elevated temperature (500°C) ultimate tensile strength values were maintained at levels exceeding those for standard AISI grades.

(15) The room temperature work hardening rates exhibited an inverse relationship with the calculated relative stacking fault energy values, further validating the trends predicted from the latter.

(16) A clear relationship was found to exist between the maximum uniform strain at room temperature and the work hardening rate.

(17) For the optimum stability alloy the combination of a low proof stress, relative to the other replacement alloys, with a high ultimate tensile strength and high work hardening rate would suggest good stretch formability characteristics for this material.

(18) Creep rupture lives for the replacement alloys were found to be rather lower than those for an AISI 347 type steel measured under similar conditions.

(19) Alloys containing Ta and (C+N) contents close to the stoichiometric ratio for Ta(C,N) showed the highest creep rupture lives.

(20) Fatigue lives for the replacement alloys were comparable with that of a similarly tested sample of AISI 316 austenitic stainless steel.

(21) Exposure of the replacement alloys with the highest and lowest Mn contents to a temperature of 750°C under a vacuum of 10^{-4} torr for 1000h resulted in a maximum depletion of manganese of 1.5% to a depth not exceeding 0.01 mm.

(22) Overall, the experimental investigations have generally confirmed the validity of the approach adopted in the design of the elementally-substituted alloys and indicate that their mechanical properties should in general be at least equivalent to those of the established steels they are designed to replace. The studies performed thus far have failed to reveal any properties that would exclude the replacement alloys from consideration as first wall or blanket materials and the generally favourable results justify further examination and development of this class of alloy.

REFERENCES

1. A.H. Bott, F.B. Pickering and G.J. Butterworth, The development of austenitic stainless steels as low-activity structural materials for fusion reactors, Culham Report CLM-R255 (1985).

2. O.N. Jarvis, Low activity materials. Reuse and disposal, Harwell Report AERE-R 10860 (1983).

3. H. Schneider, Investment casting of high hot strength 12% chrome steel, Foundry Trade Journal 108 (1960) 562.

4. E. Ruedl, D.G. Rickerby and T. Sasaki, On the role of carbon and nitrogen in austenitic Cr-Mn steels for fusion reactor structural applications, Proc. 13th Symposium on Fusion Technology, Varese, 24-28 September 1984.

5. F.R. Beckitt, The formation of sigma-phase from delta ferrite in a stainless steel, JISI 207 (1969) 632.

6. M.W. Bowkett and D.R. Harries, Martensitic transformations in cold rolled EN58 (type 321) austenitic stainless steel, Harwell Report AERE-R 9093 (1978).

7. J.A. Venables, The martensite transformation in stainless steel, Phil.Mag.7 (1962) 35.

8. F.B. Pickering, Physical Metallurgy and the Design of Steels, Applied Science Publishers, 1978.

9. BSCC High Temperature Data Book, Publ. Iron and Steel Institute, 1973.

10. R.E. Schramm and R.P. Reed, Stacking fault energies of seven commercial austenitic stainless steels, Met.Trans. 6 (1975) 1345.

11. S.R. Keown and F.B. Pickering, Effect of niobium carbide on the creep rupture properties of austenitic stainless steels, Proc. Conf. on Creep Strength in Steel and High Temperature Alloys, Sheffield, 20-27 September 1972, Publ. Met. Soc.

12. M. Snykers and E. Ruedl, Radiation damage simulation experiments on a Mn-Cr austenitic stainless steel in a HVEM, Proc 11th Symposium on Fusion Technology, Oxford, 15-19 September 1980.

13. D.J. Mazey et al, Observations of microstructure and void formation in a 8% Mn stainless steel (ICL 016) irradiated with 46 MeV nickel ions, Harwell Report AERE R-9931 (1980).

Available from
HER MAJESTY'S STATIONERY OFFICE
49 High Holborn, London, WC1V 6HB
(Personal callers only)
P. O. Box 276, London, SE1 9NH
(Trade orders by post)
13a Castle Street, Edinburgh, EH2 3AR
41 The Hayes, Cardiff, CF1 1JW
Princess Street, Manchester, M60 8AS
Southey House, Wine Street, Bristol, BS1 2BQ
258 Broad Street, Birmingham, B1 2HE
80 Chichester Street, Belfast, BT1 4JY

PRINTED IN ENGLAND